Nuclear Materials and Energy 35 (2023) 101435

Contents lists available at ScienceDirect

Nuclear Materials and Energy

journal homepage: www.elsevier.com/locate/nme

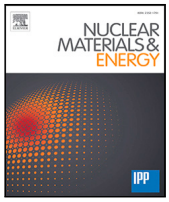

Absence of synergistic effects in quasi-simultaneous sputtering of tungsten by Ar and D ions

C. Cupak [a,*], F. Brandstätter [a], R. Cserveny [a], F. Troneberger [a], H. Biber [a], M. Fellinger [a], A. Redl [a], M.V. Moro [b], D. Böhm [c], Ch. Eisenmenger-Sittner [c], A. Mutzke [d], D. Primetzhofer [b], F. Aumayr [a]

[a] Institute of Applied Physics, TU Wien, Wiedner Hauptstraße 8-10/E134, Vienna, 1040, Austria
[b] Department of Physics and Astronomy, Uppsala University, Box 516, Uppsala, 75120, Sweden
[c] Institute of Solid State Physics, TU Wien, Wiedner Hauptstraße 8-10/E138, Vienna, 1040, Austria
[d] Max–Planck Institute for Plasma Physics, Greifswald, Wendelsteinstrasse 1, Greifswald, 17491, Germany

ARTICLE INFO

Keywords:
Tungsten
Deuterium
Argon
Sputtering yield
Mixed irradiation

ABSTRACT

A quartz crystal microbalance was used to experimentally study the erosion of tungsten during rapidly alternating bombardment with 2 keV argon and deuterium projectiles. A key goal was to investigate whether the mean sputtering yield of the alternating irradiation can be predicted from data for sputtering yields of single ion species. In addition, influences by residual gas pressure in the UHV experiment and variable ion fluxes have been studied. Our results show that the mean sputtering yield of irradiations with alternating ion species can be well predicted for a range of different fluence ratios as a simple superposition of individual sputtering yields, weighted by the respective relative fluences. This finding supports that no synergistic sputtering effects were relevant in the investigated low-flux regime.

1. Introduction

Sputtering of materials by energetic and charged atomic projectiles has a long history in applied research and many technological applications. A prominent example is the continuous surface alteration of celestial bodies without a protecting atmosphere by ions of the solar wind [1–3]. Sputtering by ion bombardment is also an important topic in nuclear fusion research. There, the first wall of nuclear fusion devices and plasma-facing components like the divertor are exposed to energetic particles from the plasma, which leads to unwanted erosion and the release of impurities into the plasma [4,5]. In industry, sputtering is employed for Physical Vapour Deposition methods (PVD) which are used to coat substrate materials of choice with thin layers of different material from the nm to the μm thickness regime [6]. Prominent applications are, for instance, coatings which improve wear-resistance [7,8] or reduce friction [9]. Direct sputtering by ion beams is also used for nano-structuring of surfaces [10,11] or to perform Focused Ion Beam (FIB) milling on the nm-scale [12].

A statistical parameter that describes sputtering is the sputtering yield, which is the mean number of sputtered target atoms per incoming projectile (the latter are often present in form of ions during experiments). Theoretical descriptions for the fundamental physical processes, which are relevant during sputtering, are established since decades [13] and literature exists in form of commonly available textbooks [14]. Also, many numerical techniques allow to simulate sputtering, e.g., with codes based on the Binary Collision Approximation (BCA) like SDTrimSP or TRIDYN [15,16] or Molecular Dynamics (MD) like PARCAS [17]. However, only few studies have focused on the question whether irradiations with multiple projectile species would cause deviations from the expected behaviour using only a single species.

From first-principle considerations, differences may occur if collision cascades in the material caused by individual ion impacts start to overlap in time, i.e., when the ion flux is sufficiently large. In this case, local dissipation of energy which is introduced by a particular projectile has not been fully completed when additional energy transfer by a subsequent projectile is deployed again. The dissipation time of a collision cascade is in the range of $t_d \sim 10^{-11}$ s or below [18–20]. Together with the expected lateral straggling of nuclear collision cascades for a given combination of projectile and target species, this allows to estimate critical fluxes above which such effects might play a role. Usually, this requires relatively high fluxes. Even for much lower fluxes, deviations could be relevant in experiments if the collision cascades overlap laterally in space, as dynamic changes of the material may occur and cause the subsequent projectiles to experience different local material properties. In this case, the total fluence of ions and the

* Corresponding author.
E-mail address: cupak@iap.tuwien.ac.at (C. Cupak).

https://doi.org/10.1016/j.nme.2023.101435
Received 20 December 2022; Received in revised form 7 March 2023; Accepted 20 April 2023
Available online 27 April 2023

lateral extension of the collision cascade are quantities which allow to estimate whether spatial overlaps are relevant for possible synergistic contributions. Also the dynamic evolution of a material's surface due to prolonged ion irradiation may change if more than a single projectile species is involved, similar as was already observed for dual beam or sequential irradiation with same ion species, but different incidence angle conditions [21–24]. This scenario could lead to a change in surface topography, which generally has a strong effect on the sputtering yield [25]. Furthermore, the surface texture (or crystallinity) may change, which is also of high relevance for predicting sputtering yields [26].

For a conventional regime where ion fluxes and fluences are low, our starting hypothesis is that the overall sputtering yield of a material during bombardment with multiple ion species can be simply described by a superposition of single ion sputtering. Here, the relative contribution may only depend on the individual ion species' fluence. Still, this hypothesis needs to be tested experimentally. Some literature on the effect of multiple ion beam irradiation (mostly with same species) exists, but focuses rather on dynamic surface pattern formation. For example, it was shown experimentally that nano-patterns formed by simultaneous irradiation with two ion beams under perpendicular azimuthal direction do not necessarily resemble patterns which are observed when the ion beams are deployed in an alternating mode [21]. This effect was also validated by means of a kinetic Monte-Carlo simulation code [27]. In addition, experiments using a linear plasma device indicated that the abundance of multiple ion species in the plasma can lead to significantly different surface modifications and variation of sputtering yields [28]. Still, at least to our knowledge, no dedicated study was conducted yet which directly investigated quantities like the sputtering yield under irradiation with more than a single ion species by using a mass-filtered, mono-energetic ion source in a low-flux and low-fluence approach. Therefore, we decided to close this gap with a dedicated series of experimental data.

For this study, we selected pure tungsten as a target material for irradiation with both Ar^+ and D_2^+ ions of 2 keV kinetic energy. This choice is motivated by nuclear fusion research, where divertor tiles are often made of tungsten. In addition, argon seeding of the deuterium–tritium plasma is an option to decrease heat loads on the divertor components and beneficial effects regarding Edge-Localised Modes (ELMs) were observed [29,30]. Thus, investigating the irradiation of tungsten with more than one ion species is relevant, since erosion of wall atoms causes a detrimental rise of the impurity level in the fusion plasma and needs to be predicted well. As a start, we aim for an experimental regime where collision cascades are not expected to overlap in time, i.e., at sufficiently low ion fluxes, to validate the applicability of a superposition principle for this case. As indicated in more detail later in the Materials and Methods section, temporally overlapping collision cascades would only become relevant for fluxes beyond 10^{26} D/(m^2·s) or 10^{28} Ar/(m^2·s), which is much higher than the technically achievable ion fluxes for our experimental setup (~10^{15} ions/(m^2·s)). Furthermore, rather low total ion fluences are aimed for to prevent surface topography changes due to sputtering. In this context, a key advantage of our highly sensitive QCM technique could be employed, which only demands low ion fluences and fluxes to precisely measure sputtering yields. Still, the intention was to apply sufficient ion fluence to achieve full spatial coverage of the sample surface with ion impacts. Therefore, local surface areas which have witnessed at least a single collision cascade should overlap in space. As shown later in the Materials and Methods section, this is the case for relatively low fluences of 10^{15} D/m^2 or 10^{17} Ar/m^2, which can be reached in short time using our setup. If any synergistic effects on sputtering are observed in this conservative regime already, this would be crucial for e.g., numerical modelling of sputtering effects utilising the BCA. In this context, we present experimental results based on irradiations with rapidly alternating ion species throughout a large number of irradiation cycles, to mimic parallel bombardment with Ar^+ and D_2^+ ions.

2. Materials and methods

The main experimental technique utilised in this study was the TU Wien Quartz Crystal Microbalance (QCM) [31–33]. Based on the principles described in the work of Sauerbrey in 1959 [34], very small mass changes Δm of a quartz crystal resonator can be deduced from its recorded eigenfrequency change Δf. This connection is formulated in Eq. (1), which also includes the initial quartz crystal mass m_0 and eigenfrequency f_0, respectively.

$$\frac{\Delta m}{m_0} = -\frac{\Delta f}{f_0} \tag{1}$$

At TU Wien, dedicated electronic components and SC-cut quartz resonators allow to achieve a high sensitivity in real time (~10 pg/cm^2/s) during our experiments. The connection between frequency and mass still holds if a thin layer of different material is applied on top of the resonator, like for instance W. This is especially useful, e.g., for investigation of sputtering due to impinging ions. More information can be found in Refs. [31,32].

In this study, a layer of pure W was applied on a quartz crystal resonator with an approximate thickness of 500 nm by means of DC magnetron sputtering at the Institute of Solid State Physics at TU Wien. To achieve satisfactory film growth and to prevent delamination, the resonators were heated to a temperature of ~470 K. A commercial 4“ W sputter target with a nominal purity of 99.99 wt% was chosen for the deposition. It was mounted into a magnetron sputter source, operated in an argon atmosphere of 4×10^{-3} mbar and at a power of 300 W. As a result, the coated quartz crystal resonators obtained a mirror-like surface finish. After production, the W coated quartz crystal was investigated by means of an Atomic Force Microscope (AFM). A very flat surface topography was validated with a Root-Mean-Square (RMS) roughness of 2.2 nm. Since the mean inclination angle δ_m was found to be an important roughness parameter concerning sputtering [25], is was also extracted from our AFM data with a value of δ_m ~10.2°. Both the low RMS and δ_m value support that for the sputtering experiments in this study, no significant effects from surface roughness are *a-priori* relevant [25]. Furthermore, the overall erosion as estimated from total fluences applied in the main experiments did not exceed 3.5 nm, therefore no significant changes of the surface roughness were expected. Besides surface roughness, also the composition of the sample was checked by *ex-situ* ion beam analysis methods [35] (Rutherford Backscattering and Time-of-Flight/Energy Elastic Recoil Detection Analysis) at the Tandem accelerator laboratory in Uppsala, Sweden [36]. Apart from small surface contaminations in the nm-thickness range, a clean W film with approximately 98 at.% purity was validated.

The quartz crystal sample was mounted on a 4-axes manipulator inside our UHV experiment, which achieves base pressures in the 10^{-10} mbar range and maintains low levels of 10^{-8} mbar during ion bombardment. This rise of pressure is due to the inevitable influx of working gas from the ion source, which affects also the experimental chamber section although differential pumping stages were implemented. Prior to the measurements, Ar sputter cleaning of the sample surface was performed to remove adsorbates from atmospheric exposition. Ion generation was achieved by a commercial SPECS IQE 12/38 ion source, which was equipped with a Wien-filter to select ions with a specific q/m ratio. In this study, the ion source was supplied with working gas which was mixed with a desired composition of Ar and D_2 in a mixing volume. We furthermore used an ISEG ZP001 high voltage Wien-filter module to enable remote control and deflection voltage adjustment for the Wien-filter hardware with a PC, which thus allowed us to quickly switch between different ion species generated from the ion source. This way, we could obtain sample irradiation in a quasi-concurrent pattern with two ion species using only one ion source. In the course of this study, 2 keV Ar^+ and 2 keV D_2^+ ions were used as projectiles under 0° incidence angle relative to the surface normal. Typical ion fluxes (measured with a Faraday-cup) were 8.5×10^{15} Ar/m^2/s and 9.7×10^{15}

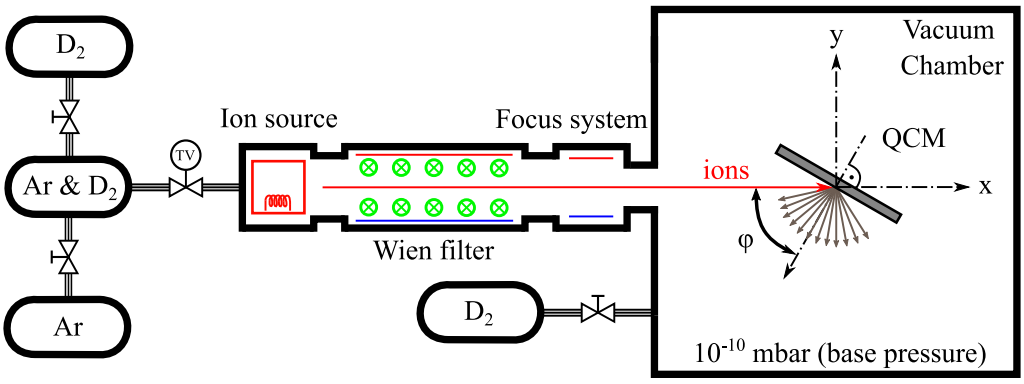

Fig. 1. Schematic of the experimental setup. A SPECS IQE 12/38 ion source was operated at 2 kV acceleration voltage with a mix of Ar and D_2 working gas (influx controlled with a thermo-valve (TV)), while a PC-controlled Wien-filter allowed to select a specific ion species with defined q/m ratio and kinetic energy for QCM sample irradiation. The QCM sample position and rotation ($\phi = 0°$ in this study) was set with a 4-axis manipulator, which also allowed to position a Faraday-cup (FC) for ion flux measurement.

$D_2/m^2/s$, respectively. Fig. 1 shows a simplified sketch of the utilised experimental setup. Even though both projectile species were extracted at the same kinetic energy, their difference in mass leads to much different sputtering yields. Furthermore, the expected ion ranges in W are different. In Fig. 2, projectile ranges can be inspected for the individual species in W as calculated with the BCA code SDTrimSP [15], using a recently developed GUI interface [37]. The mean ion ranges r_{ion} for 2 keV Ar and 1 keV D (which mimics molecular D_2 irradiation at 2 keV) were 23.7 Å and 150 Å, respectively. These quantities can be used as an upper limit for the lateral straggling, which in turn allows to calculate the laterally projected area occupied by a collision cascade using r_{ion}^2. The reciprocal value $1/r_{ion}^2$ then corresponds to an estimative value for the fluence necessary to cover (in average) the whole area of a sample surface at least once with collision cascades. If furthermore the energy dissipation time t_d of a collision cascade is considered ($\sim 10^{-11}$ s, see [18]) using $1/(r_{ion}^2 \cdot t_d)$, an estimation for the necessary fluxes can be obtained, where also temporally overlapping collision cascades would be relevant. Regarding the critical fluxes for temporally overlapping collision cascades, 1.8×10^{28} Ar/(m^2·s) and 2.2×10^{26} D_2/(m^2·s) would be necessary, which exceeds the capabilities of our experiment by orders of magnitudes. Therefore, studying effects from temporally overlapping collision cascades was never possible, nor intended in this experimental study. However, since only low ion fluxes are applied in this work, it allows to assume that in comparison to a purely parallel setup with two individual ion sources, no difference was introduced by quickly alternating the ion species during irradiation, as a temporal overlap in collision cascades is not relevant in this regime.

A Faraday-cup (FC) was used to precisely quantify individual ion fluxes prior and after each experiment. These data were used for the evaluation of sputtering yields, while the error in the ion flux was the most relevant contributor to the calculated error in the sputtering yield. By knowledge of individual ion fluxes, also a certain fluence ratio between the ion species could be achieved by switching between the corresponding Wien-filter deflection voltages, following desired irradiation step times. We define the fluence ratio R by division of the Ar fluence Γ_{Ar} over the total fluence for all ion species, $\Gamma_{Ar} + \Gamma_{D_2}$, as defined in Eq. (2).

$$R = \frac{\Gamma_{Ar}}{\Gamma_{Ar} + \Gamma_{D_2}} \tag{2}$$

Fig. 3 shows a schematic ion current pattern when measured with the Faraday-cup. For visualisation purposes, step times of 10 s for Ar^+ and 20 s for D_2^+ were set respectively. During the actual measurements, these times were adjusted to meet fluence ratios more relevant for the divertor region of fusion devices (where seeding gas concentrations in the at.% range are expected). We were able to precisely control the irradiation step times with an absolute error below 0.05 s.

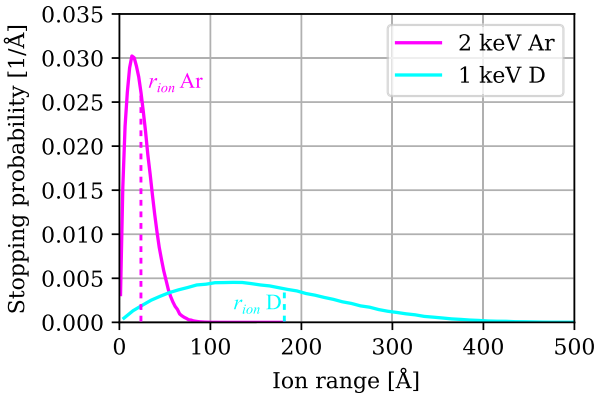

Fig. 2. Range of 1 keV D and 2 keV Ar projectiles in W for irradiation along the surface normal direction. Also the mean ion range r_{ion} is added for the individual projectiles. The data was obtained using the SDTrimSP code [15,37].

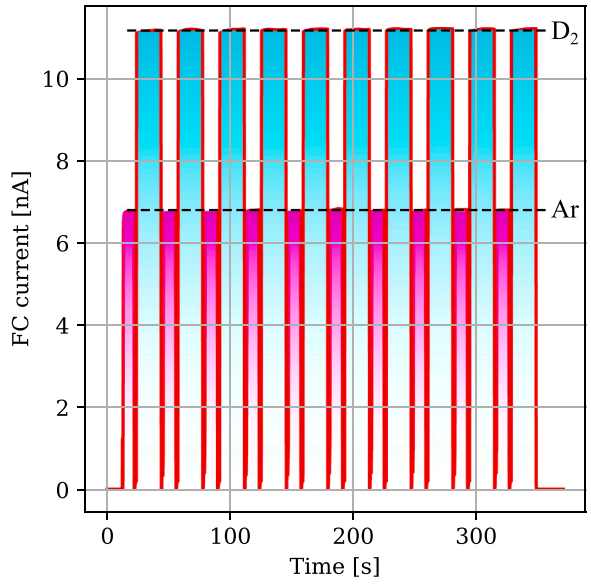

Fig. 3. Signal of the FC during alternating irradiation with focused Ar^+ and D_2^+ ions. In total, 10 steps of each ion species are shown here for visualisation. In this specific case, the Ar^+ beam had a stable intensity of 6.7 nA and a defined step time of 10 s (magenta), while the D_2^+ beam had an intensity of 11.1 nA and 20 s step time (cyan). The desired step times could be set with an absolute error below 0.05 s, which was therefore neglected when calculating fluence ratios. (For interpretation of the references to colour in this figure legend, the reader is referred to the web version of this article.)

In the course of this study, three different fluence ratios close to the at.% regime were inspected. To mimic a long-term irradiation with simultaneous Ar^+ and D_2^+ impact on our sample, many of such Ar^+ & D_2^+ cycles (usually 100) were performed. This procedure caused a characteristic QCM signal response as shown later in Fig. 4. Typical total fluences (including both species) per experiment were on the range of 10^{21} ions/m^2, which demanded total irradiation times of up to two days. The sputtering yield for the mixed ion irradiation was finally deduced from the absolute frequency change as measured by the QCM during the long-term bombardment with alternating Ar^+ & D_2^+ irradiation. This value was divided by the overall fluence of both ion species applied in this regime. Prior to any of the alternating experiments, the sample was furthermore irradiated with pure 2 keV D_2^+ ions up to a sufficiently large fluence. This pre-irradiation was conducted to ensure saturation of D implantation, which could be validated in-situ by a stationary frequency slope signal of the QCM. Such a regime allows to attribute mass changes solely to sputtering [3].

Due to inevitable but small variations of the ion beam flux over the experimental period, a small deviation from the initially set fluence ratio was possible and therefore cross-checked by Faraday-cup data measured after each experimental cycle. This enabled to re-calculate the actual fluence ratio R_a, while almost no difference to the initially set values was observed.

Each mixed Ar^+ and D_2^+ measurement was accompanied with single ion irradiations to gain sputtering yield data as a reference (more details in Section 3). This was performed prior to and after the alternating irradiations, enabling to identify eventual dynamic changes. The resulting sputtering yield data from these reference measurements were further used to calculate an estimated sputtering yield for the alternating irradiations, as expected from an analytical formula (see Eq. (3)), which takes into account the measured fluence ratios R.

$$Y_a = Y_{r,Ar} \cdot R + Y_{r,D_2} \cdot (1 - R) \tag{3}$$

Eq. (3) is directly derived from our initial hypothesis, that sputtering with mixed ion species can be seen as a simple superposition of single ion irradiations within our selected regime of flux and fluence. Gaussian error propagation was applied on Eq. (3) to assess the error in the predicted quantities, which mostly depended on the error of reference sputtering yields and the error in the fluence ratio.

It has to be mentioned that for the reference measurements, all experimental conditions were kept exactly the same as for the alternating Ar^+ & D_2^+ irradiations. This was especially of importance for the total pressure during operation (dominated by the mix of Ar and D_2 working gas) and the ion fluxes in our experiment. If these parameters change, we observed that sputtering yields can significantly differ, which points towards a contribution of adsorbate-related effects. As shown in the Appendix, we observed that the sputtering yield of molybdenum, e.g., drops to lower values if higher residual gas pressure and lower ion fluxes are chosen. During 2 keV D_2^+ irradiation with a flux of 3.9×10^{15} $D_2/m^2/s$, we found a significant effect when D_2 background pressure was increased from 1.2×10^{-8} mbar to 5×10^{-7} mbar, causing the sputtering yield to decrease to 38% of the initial value (for details, see Appendix). Our explanation is the presence of a certain surface adsorbate coverage, which is relevant even during ion irradiation in steady-state conditions, where the impingement flux and sticking from residual gas atoms is equilibrating the flux of sputtered adsorbate atoms from the sample surface. The equilibrium adsorbate coverage may act as additional surface barrier, which prevents some of the underlying target atoms from being sputtered. Effects on sputtering yields introduced by surface contamination were also reported in literature [38–40]. It was therefore found to be an important boundary condition to maintain chamber pressure, working gas mixture and ion flux throughout the experimental campaign, to enable comparison of predicted and measured sputtering yields and especially the application of Eq. (3).

3. Results and discussion

As a first result, a general overview on the frequency data as recorded by the QCM during a representative measurement with alternating ion species can be seen in Fig. 4 (exemplary for R_a = 1.99 at.% in this case). As mentioned in the previous section, also reference sputtering yield measurements for single ion irradiation were performed prior and after the alternating Ar^+ & D_2^+ phase (indicated by Ar or D_2 in Fig. 4 left). For these reference measurements, special care was taken to reach steady-state conditions, e.g., a constant slope of the time-dependent frequency signal, which was then considered for sputtering yield determination. This ensured quasi-stationary conditions, e.g., initial dynamics from remaining implantation processes, temperature variations, or changes in adsorbate coverages equilibrated, leading to linear trends in the data. In Fig. 4 (right), the recorded frequency signal from the QCM during alternating irradiations can be observed in more detail, revealing a step-like picture. While the overall tendency during alternating irradiation followed a linear trend indicating stationary conditions, small temporal deviations from a constant slope can be observed for the individual irradiation steps. Furthermore, the average frequency slopes are different for the Ar^+ and D_2^+ irradiations in the mixed case when compared to the reference measurements with single ion irradiation. This phenomenon is especially visible for the D_2^+ steps in Fig. 4 (right), where even negative frequency slopes are observable. Such a trend is indicating a positive mass change, which is principally not expected during sputtering and requires further investigation. To support the methodology in this study, these data are discussed in detail to identify the cause for this signal evolution during the step-wise irradiation. The frequency slopes during the reference measurements $\dot{f}_r$ and the average short-term values for the Ar^+ and D_2^+ steps $\dot{f}_{step}$ are listed in Table 1 using data from the representative case shown in Fig. 4. In addition, also the difference between these frequency slopes (or residual frequency slopes) is listed in column 3 as $\dot{f}_{res}$, which therefore represents a mass change signal which cannot be attributed to tungsten sputtering as during the reference cases. Column 4 includes information on the irradiation step time t_s for the relevant ion species, while the last column indicates the product of step time with the residual frequency change, indicated by Δf_{res}. It can be observed, that the latter values are practically identical except for their sign, which indicates that a small extra mass gain during D_2^+ irradiation is perfectly equilibrated by a corresponding mass loss during the subsequent Ar^+ irradiation step. One potential hypothesis is that these dynamic, but globally equilibrating effects are again related to the contribution of (periodically varying) surface adsorbate coverages. The residual frequency change Δf_{res} can be expressed as a mass change of 8.35×10^{18} amu/m^2, which may be interpreted as 4.15×10^{18} D/m^2, which approximately matches the required surface coverage for a monolayer. This can be put into relation with the fluence applied during a short Ar^+ step, which was 1.68×10^{17} Ar/m^2. Therefore, average adsorbate sputtering yields of 49.62 amu/Ar or 24.64 D/Ar can be deduced, if Δf_{res} is connected to a variable adsorbate coverage. Adsorbate effects are generally discussed in more detail in the Appendix of this manuscript. Another hypothesis for the origin of these periodic fluctuations in Δf_{res} is related to an interplay between implantation and Ar-beam enhanced mobilisation and outgassing of D. In this scenario, a surface-near part of the implanted D is emitted during the Ar^+ steps (as the range of Ar^+ is relatively short), which is followed by re-implantation of D into the empty trapping reservoirs during the subsequent D_2^+ irradiation. Thus, the enhanced outgassing and the re-implantation of D may equilibrate in average, which can explain the recorded frequency signal. In this case, approximately 24% of the fluence applied per D_2^+ step would be re-implanted in the reservoir which was released during the previous Ar^+ step.

Since the QCM only allows to measure net mass changes, no clear answer to the real origin of this interplay can be presented in the course of this study. However, since the global trend in the frequency

Table 1
Comparison of frequency slopes during reference measurements and stepwise irradiations in the mixed Ar^+ & D_2^+ case. The product of step time and residual frequency change practically equilibrates between subsequent Ar & D_2 steps (Δf_{res}).

Case	$\dot{f}_r$ [Hz/min]	$\dot{f}_{step}$ [Hz/min]	$\dot{f}_{res}$ [Hz/min]	t_s [min]	Δf_{res} [Hz]
Ar	+1.2000	+1.5060	+0.3060	0.33	+0.102
D_2	+0.0059	−0.0014	−0.0073	14.25	−0.104

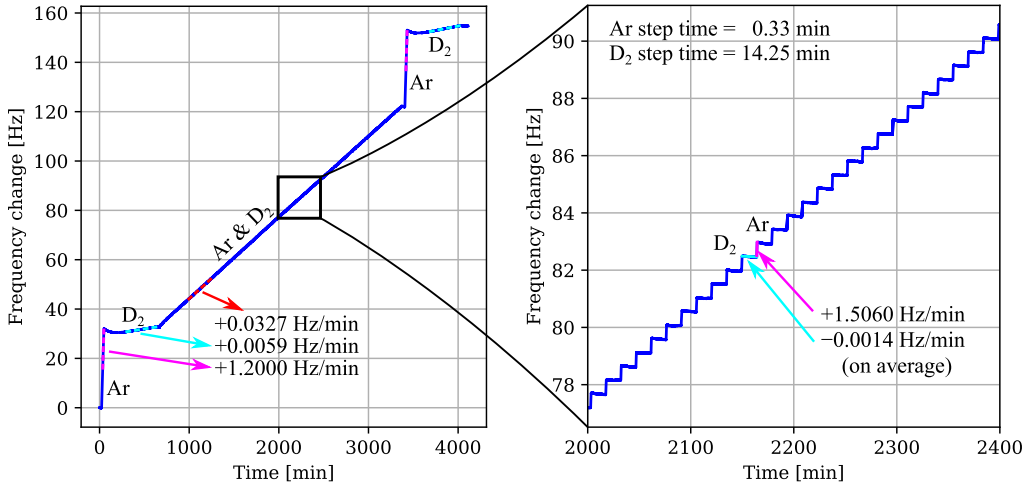

Fig. 4. Representative QCM signal during a measurement with fluence ratio R_a = 1.99 at.%. The frequency change is plotted over time. Frequency increase corresponds to a decrease in mass, according to Eq. (1). **Left:** The whole measurement is displayed with the individual phases of Ar^+, D_2^+, or mixed ion irradiation. **Right:** The inset shows the QCM measured frequency response during alternating Ar^+ & D_2^+ irradiation in more detail.

evolution was not affected, a determination of the sputtering yield assuming quasi-stationary conditions could be well obtained from the alternating Ar^+ & D_2^+ measurements. The same phenomenon were relevant for all fluence ratio cases.

In the following, sputtering yield data for all investigated cases with individually set fluence ratios are presented and discussed. The results are summarised in Table 2. The first column denotes the actual fluence ratio R_a as derived from both a-priori and a-posteriori Faraday-cup measurements. For each experimental case, reference sputtering yields of pure 2 keV Ar^+ and D_2^+ irradiation ($Y_{r,Ar}$ and Y_{r,D_2}) are listed in the second and third column. These values were used as input for the calculation of sputtering yields for the mixed Ar^+ & D_2^+ irradiation, according to the analytical Eq. (3). The resulting values $Y_{m,a}$ can be found in the fourth column, and can be compared with the values directly measured during the mixed Ar^+ & D_2^+ experiments ($Y_{m,e}$) in the last column.

First of all, the values of the reference sputtering yields are discussed. The data for $Y_{r,Ar}$ are consistent for all investigated fluence ratio cases (with deviations only in the second digit). Similarly, this is also observable for Y_{r,D_2}, even though the data appear slightly more scattered. Still, all values agree within their error bars. It has to be mentioned, that the D_2^+ sputtering yields are a factor of about 200 smaller than the Ar-based sputtering yields and therefore more challenging to determine experimentally.

Finally, for the mixed irradiation case, the analytical sputtering yields $Y_{m,a}$ and the experimentally deduced values $Y_{m,e}$ are compared. For each experimental case, these values match well and deviate only within the range of their error bars. It can be observed that the sputtering yields decrease for lower fluence ratios, which is caused by the increasing contribution of D_2^+ to the overall fluence. Therefore, the sputtering yields propagate towards the level of pure D_2^+ irradiation. Still, the effect of Ar^+ to the sputtering is always significant. In addition, the calculated sputtering yield values $Y_{m,a}$ are always slightly higher than $Y_{m,e}$. This fact can probably be explained by different surface coverages with adsorbates for the case of pure Ar^+ or D_2^+ irradiation, and the individual phases during mixed Ar^+ & D_2^+ bombardment. Still, the final results regarding the sputtering yield of mixed ion irradiation

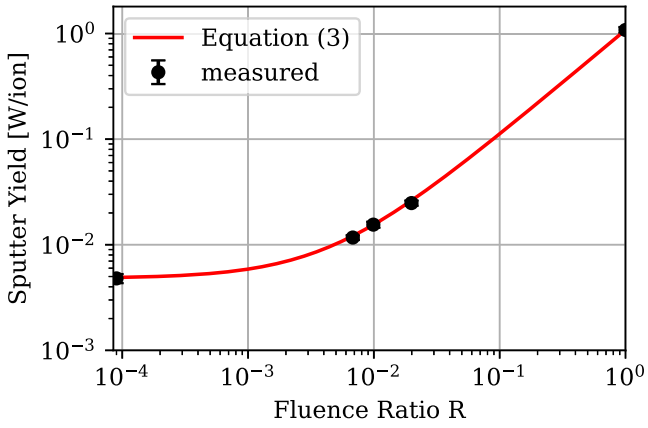

Fig. 5. W sputtering yields for mixed Ar^+ and D_2^+ irradiation at 2 keV kinetic energy, as a function of the fluence ratio R. The measured values (black data points) are compared with predicted sputtering yields (red) using Eq. (3). A double-logarithmic scale is used. The data point close to $R = 10^{-4}$ corresponds to the asymptotic case $R = 0$. (For interpretation of the references to colour in this figure legend, the reader is referred to the web version of this article.)

are in very good agreement with the predicted values, which therefore indicates that these effects were sufficiently small to enable such an approach. To further visualise this, the measured data regarding $Y_{m,e}$ from Table 2 and predicted values from the analytic Eq. (3) are presented in Fig. 5 in a double-logarithmic plot. Here, only the reference sputtering yields $Y_{r,Ar}$ and Y_{r,D_2} were used as carrier points for the asymptotic cases $R = 0$ ($\sim 10^{-4}$ in the plot) and $R = 1$, but no fitting of the calculated values was performed.

The utilisation of Eq. (3) was based on the hypothesis, that the sputtering yield of mixed ion irradiations can be calculated by a superposition of sputtering yields for single ion irradiations, weighted by their relative fluence contribution. Based on the good agreement, we could validate that this is indeed the case. Thus, there are no synergistic effects to be expected when sputtering of surfaces is performed with

Table 2
Measured sputtering yield data (in W atoms per ion) for the investigated cases with variable fluence ratios. The errors are mostly due to the experimental uncertainty in the measured ion flux.

R_a	$Y_{r,Ar}$ [W/ion]	Y_{r,D_2} (10^{-3}) [W/ion]	$Y_{m,a}$ (10^{-2}) [W/ion]	$Y_{m,e}$ (10^{-2}) [W/ion]
1.99%	1.05 ± 0.06	4.83 ± 0.47	2.56 ± 0.24	2.48 ± 0.14
1.01%	1.09 ± 0.07	4.67 ± 0.23	1.57 ± 0.14	1.55 ± 0.10
0.68%	1.10 ± 0.06	4.91 ± 0.24	1.23 ± 0.09	1.17 ± 0.06

different ion species at once, at least not for our studied range of experimental parameters (in particular for comparable low ion fluxes).

In this study, we used a remotely controlled Wien-filter with a single ion source to mimic parallel irradiation with two ion species by performing an alternating irradiation pattern. While it was already argued in the introduction that in our studied flux regime no differences are to be expected, future studies using two independent ion sources would still be favourable. Such an approach would be interesting since it has been observed that for higher fluences and irradiations under grazing ion incidence angles, nano-patterns which formed during dynamic erosion appeared different between sequential and parallel bombardment cases [21]. Furthermore, we observed contributions which we attribute to a certain surface adsorbate coverage, being relevant even during ion irradiation (see Appendix). Therefore, future experiments can focus on the creation of better base pressures and/or higher ion fluxes during the measurements, since both will reduce the surface adsorbate coverage.

4. Summary and conclusion

In the course of this study, an alternating irradiation with 2 keV Ar^+ and D_2^+ ions was performed to experimentally investigate the effect of mixed ion bombardment on sputtering yields of a W surface by means of a quartz crystal microbalance. We compared the measured sputtering yields with values derived from a superposition of sputtering yields for pure ion bombardment weighted with the respective fluence ratios to predict the sputtering yield of the mixed irradiation.

Generally, we observed that it was crucial to precisely maintain a low base pressure and stable ion fluxes throughout our measurement campaign. We attribute this to the contribution of a certain surface adsorbate coverage relevant even during ion irradiation, which acts similar to an additional surface barrier and prevents a part of the target atoms from being sputtered. This can be a challenging limitation also for many other experiments, since the pressure during operation was already comparably low in our case (~10^{-8} mbar). As long as the pressure and ion flux conditions were kept constant, we observed no significant differences between predicted and measured sputtering yield values for the mixed Ar^+ & D_2^+ cases. Therefore, we conclude that the fundamental approximation of a simple superposition law can be well justified, which furthermore implies that within our investigated regime of experimental conditions, there are no substantial synergistic effects to be expected when irradiating with more than a single ion species.

CRediT authorship contribution statement

C. Cupak: Conceptualization, Methodology, Investigation, Data curation, Formal analysis, Visualization, Writing – original draft, Writing – review & editing. **F. Brandstätter:** Data curation, Investigation, Writing – review & editing. **R. Cserveny:** Data curation, Investigation, Writing – review & editing. **F. Troneberger:** Data curation, Investigation, Writing – review & editing. **H. Biber:** Conceptualization, Formal analysis, Methodology, Writing – review & editing. **M. Fellinger:** Formal analysis, Writing – review & editing. **A. Redl:** Software, Writing – review & editing. **M.V. Moro:** Investigation, Data curation, Writing – review & editing. **D. Böhm:** Resources, Writing – review & editing. **Ch. Eisenmenger-Sittner:** Resources, Writing – review & editing. **A. Mutzke:** Software, Writing – review & editing. **D. Primetzhofer:** Formal analysis, Funding acquisition, Writing – review & editing. **F. Aumayr:** Conceptualization, Methodology, Formal analysis, Funding acquisition, Supervision, Writing – review & editing.

Declaration of competing interest

The authors declare that they have no known competing financial interests or personal relationships that could have appeared to influence the work reported in this paper.

Data availability

Data will be made available on request.

Acknowledgements

This work has been carried out within the framework of the EUROfusion Consortium, funded by the European Union via the Euratom Research and Training Programme (Grant Agreement No 101052200—EUROfusion). Views and opinions expressed are however those of the author(s) only and do not necessarily reflect those of the European Union or the European Commission. Neither the European Union nor the European Commission can be held responsible for them. Financial support has also been provided by KKKÖ (commission for the coordination of fusion research in Austria at the Austrian Academy of Sciences - ÖAW). Support of the operation of the tandem accelerator at Uppsala University, Sweden by VR-RFI (contract #2019-00191) is gratefully acknowledged. We are furthermore thankful for the coating of QCM crystals with molybdenum by M. Oberkofler (Max Planck Institute of Plasma Physics, Garching, Germany). The authors also acknowledge TU Wien Bibliothek for financial support through its Open Access Funding Programme.

Appendix. Influence of adsorbates

The results in the main manuscript require a more in-depth discussion of the relevant contributions to sputtering which can be expected from adsorbate layers on top of surfaces under ion irradiation. Generally, it is already well known that sputtering yield measurements depend on the surface condition of a specimen, i.e, whether it is clean or covered with adsorbates or oxides [38–41]. Also hydrogen isotopes are well capable of forming adsorbate layers on metals, as a large number of studies has already shown (e,g., [42–44] and references therein). Since literature on this topic exists, only some aspects relevant for our work are shortly recapitulated. In Fig. A.6, a simplified sketch including individual in- and outgoing particle fluxes is displayed for ion bombardment of a substrate material covered by adsorbates. If no ion beam hits the surface, the steady-state adsorbate layer coverage is dependent only on the influx and sticking of adsorbates $\Phi_{ad,ad}$, and the outflux due to thermal desorption $\Phi_{ad,des}$. Assuming an ideal gas in the experimental chamber, the influx $\Phi_{ad,ad}$ is proportional to the impingement rate of residual gas atoms with a certain mean velocity $\bar{v}$ at a given temperature T and pressure p [45], and also proportional to a sticking coefficient s (see Eq. (A.1)).

$$\Phi_{ad,ad} \sim \frac{p \cdot \bar{v}}{4 \cdot k_b \cdot T} \cdot s \tag{A.1}$$

The sticking coefficient is expected to decrease for increasing adsorbate layer thickness, otherwise the adsorbate layer would grow infinitely. Furthermore, sticking for gases like D_2 is expected to be higher than for noble gases like Ar, due to its chemical reactivity.

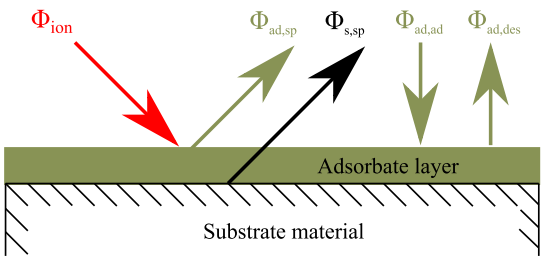

Fig. A.6. Simplified sketch of a substrate material with a top adsorbate layer under ion irradiation. In steady-state conditions, the surface adsorbate coverage is constant and the influx of adsorbate atoms $\Phi_{ad,ad}$ due to sticking of residual gas atoms is balanced by the outflux from thermal desorption $\Phi_{ad,des}$ and sputtering $\Phi_{ad,sp}$. The outflux of sputtered substrate atoms $\Phi_{s,sp}$ is expected to depend on the surface adsorbate coverage.

As described by P.A. Redhead in 1962, the reduction path by thermal desorption is featuring an Arrhenius-type energy dependence [46], as shown in Eq. (A.2).

$$\Phi_{ad,des} \sim e^{-\frac{E_{b,ad}}{k_b \cdot T}} \tag{A.2}$$

In Eq. (A.2), the parameter $E_{b,ad}$ stands for the binding energy of adsorbates. A multitude of binding sites can be expected for adsorption on a metal surface, which result in various binding energies [42]. Under ion bombardment, an additional reduction path is introduced, which can be calculated by the incoming ion flux times the sputtering yield for the present adsorbate coverage, as stipulated in Eq. (A.3).

$$\Phi_{ad,sp} = Y_{ad} \cdot \Phi_{ion} \tag{A.3}$$

For higher adsorbate sputtering yields Y_{ad} due to favourable kinetics, the steady-state adsorbate layer thickness can be reduced more efficiently and the substrate becomes cleaner, i.e., supporting the assumption that our surface is cleaner under Ar than during D_2 irradiation. It has to be mentioned that the sputtering yield of adsorbates will generally decrease if the adsorbate coverage is getting lower, as the chance for interaction with adsorbate particles decreases. The impinging ion beam also sputters the substrate, while the flux of sputtered substrate atoms $\Phi_{s,sp}$ is reduced for higher adsorbate coverage, which corresponds to a lower substrate sputtering yield. Following the argumentation by Gruen et al. this effect is probably connected to "shadowing" of the substrate by the top adsorbate layers [39].

Summarising, the sputtering yield of the substrate material can be expected to be smaller for increasing residual gas pressures and decreasing ion beam fluxes, since a certain surface adsorbate coverage may remain even during steady-state irradiation conditions.

To complement these basic assumptions, the influence of D_2 residual gas pressure on sputtering yields was tested for a molybdenum coated quartz crystal under 2 keV Ar^+ and 2 keV D_2^+ bombardment at 0° ion incidence (perpendicular to the surface). Similar as for the reference measurements on tungsten, the same setup as described in the main part of the manuscript was used. The only difference was the utilisation of a leak valve, which was enabling an additional increase of D_2 residual gas pressure in the vacuum chamber, while the ion source maintained the same flux of ions. For the Ar^+ case, a flux of 5.3×10^{15} $Ar/m^2/s$ was set, while for D_2^+, a flux of 3.9×10^{15} $D_2/m^2/s$ was achieved. The sample was continuously irradiated while the mass loss was measured with the QCM. The pressure was increased step-wise and the corresponding sputtering yield was deduced during steady-state conditions (e.g., where a constant frequency slope indicated that all dynamic changes had settled). It should be mentioned, that for these pressures, the impingement rate of D_2 molecules is already on the same order of magnitude as the ion fluxes in our experiments (ranging from 9.23×10^{16} $D_2/(m^2 \cdot s)$ for 1.2×10^{-8} mbar up to 7.69×10^{18} $D_2/(m^2 \cdot s)$ for 1.0×10^{-6} mbar). However, no significant interaction between the incoming ion beam and residual gas atoms is yet expected, as the mean free path of the latter is on the range of 100 m to 10 km, depending on the individual pressure case. The data is summarised in Tables A.3 and A.4.

A clear trend was observed in both irradiation cases. For increasing chamber pressure (first column), the sputtering yields dropped to lower values (second column, relative decrease in the third column). In agreement to the basic assumptions introduced above, our explanation for this behaviour is pointing towards a dependence of the molybdenum sputtering yield on the adsorbate coverage on top of the sample.

To complement these experimental findings, a set of simulations was conducted with the BCA code SDTrimSP in combination with a recently developed graphical user interface [15,37]. Similar as for the approach followed by Pellin et al. using the TRIM code [47], we tried to mimic the sputtering behaviour of our sample by tuning available input parameters. On the one hand, the presence of a surface adsorbate coverage appears to act like an additional surface barrier, which prevents a part of the sputtered molybdenum atoms from escaping. Starting from the standard surface binding energy for molybdenum of 6.81 eV, a substantial increase was necessary to match the sputtering yields measured in the experiment with SDTrimSP (see fourth column of Tables A.3 and A.4). The necessary increase was higher for D_2 than for Ar irradiation. Another approach to simulate the scenario was to directly implement a top D_2 adsorbate layer with a virtual thickness d_{ads} in SDTrimSP. In this case, the surface binding energies of Mo and D_2 were kept to default values, but the thickness was varied until a match between the experimental and simulated sputtering yields of Mo was obtained (see fifth column). For both ion irradiation cases, a continuous increase of the virtual adsorbate layer thickness was necessary to reconstruct the Mo sputtering yields at rising background pressures. Again, the D_2 case demanded more severe manipulation, i.e., thicker adsorbate layers, than the Ar case. This observation is in line with our basic assumptions above, supporting the hypothesis that the presence of a certain surface adsorbate coverage was indeed affecting the Mo sputtering yields during the measurements at elevated D_2 pressures. It has to be mentioned that these SDTrimSP simulations where only conducted with the purpose to show the effects caused by adsorbate coverages qualitatively, while a precise prediction of realistic adsorbate behaviour may require more careful implementation.

Comparing the data in Tables A.3 and A.4, it has to be assumed that some adsorbate coverage was relevant even for the lowest pressure during our experiments. Therefore, it was also of high importance to always maintain the same residual gas pressures and ion fluxes for all measurements presented in the main part of this manuscript. Otherwise, the measured reference sputtering yields would not have enabled a direct comparability to predict sputtering yields of the alternating Ar & D irradiations. It has to be mentioned, that the QCM technique solely enables to measure net mass changes and our experiments did not allow to investigate the composition or abundance of adsorbates directly.

Table A.3
Summary of sputtering yield data for 2 keV Ar^+ irradiation of a Mo coated QCM sample at variable D_2 residual gas pressure. SDTrimSP was used to reconstruct the measured sputtering yields either by tuning the surface binding energy E_b or by inclusion of an adsorbate layer of certain thickness d_{ads}.

Pressure (mbar)	Sp. yield (Mo/Ar)	Rel. decrease	E_b [eV]	d_{ads} [Å]
1.2×10^{-8}	1.31 ± 0.17	–	9.81	8
5.0×10^{-7}	1.28 ± 0.16	2.3%	10.06	9
1.0×10^{-6}	1.08 ± 0.13	17.6%	11.68	12

Table A.4
Summary of sputtering yield data for 2 keV D_2^+ irradiation of a Mo coated QCM sample at variable D_2 residual gas pressure. SDTrimSP was used to reconstruct the measured sputtering yields either by tuning the surface binding energy E_b or by inclusion of a adsorbate layer of certain thickness d_{ads}.

Pressure (mbar)	Sp. yield (10^{-3} Mo/D_2)	Rel. decrease	E_b [eV]	d_{ads} [Å]
1.2×10^{-8}	17.6 ± 1.3	–	11.88	14
5.0×10^{-7}	6.7 ± 0.4	61.8%	18.43	29

Furthermore, the relevance of adsorbate effects is only assumed to be significant in the case of a residual gas composition dominated by chemically active species (e.g., D_2), while it might be neglectable for experiments utilising noble gases due to a much lower sticking coefficient.

References

[1] P. Wurz, S. Fatemi, A. Galli, J. Halekas, Y. Harada, N. Jäggi, J. Jasinski, H. Lammer, S. Lindsay, M.N. Nishino, T.M. Orlando, J.M. Raines, M. Scherf, J. Slavin, A. Vorburger, R. Winslow, Solar wind Helium ion interaction with Mg and Fe rich pyroxene as Mercury surface analogue, Space Sci. Rev. 218 (2022) 10.

[2] P.S. Szabo, H. Biber, N. Jäggi, M. Wappl, R. Stadlmayr, D. Primetzhofer, A. Nenning, A. Mutzke, J. Fleig, K. Mezger, H. Lammer, A. Galli, P. Wurz, F. Aumayr, Experimental insights into space weathering of phobos: Laboratory investigation of sputtering by atomic and molecular planetary ions, J. Geophys. Res. Planets 125 (2020) e2020JE006583.

[3] H. Biber, P.S. Szabo, N. Jäggi, M. Wallner, R. Stadlmayr, M. Moro, A. Nenning, A. Mutzke, K. Metzger, H. Lammer, D. Primetzhofer, J. Fleig, A. Galli, P. Wurz, F. Aumayr, Solar wind Helium ion interaction with Mg and Fe rich pyroxene as Mercury surface analogue, Nucl. Instrum. Methods Phys. Res. B. 480 (2020) 10–15.

[4] S. Brezinsek, A. Kirschner, M. Mayer, A. Baron-Wiechec, I. Borodkina, D. Borodin, I. Coffey, J. Coenen, N. den Harder, A. Eksaeva, C. Guillemaut, K. Heinola, A. Huber, V. Huber, M. Imrisek, S. Jachmich, E. Pawelec, M. Rubel, S. Krat, G. Sergienko, G. Matthews, A. Meigs, S. Wiesen, A. Widdowson, JET contributors, Erosion, screening, and migration of tungsten in the JET divertor, Nucl. Fusion 59 (2019) 096035.

[5] C. Linsmeier, M. Rieth, J. Aktaa, T. Chikada, A. Hoffmann, J. Hoffmann, A. Houben, H. Kurishita, X. Jin, M. Li, A. Litnovsky, S. Matsuo, A. von Müller, V. Nicolic, T. Palacios, R. Pippan, D. Qu, J. Reiser, J. Riesch, T. Shikama, R. Stieglitz, T. Weber, S. Wurster, J.-H. You, Z. Zhou, Development of advanced high heat flux and plasma-facing materials, Nucl. Fusion 57 (2017) 092007.

[6] D.M. Mattox, Handbook of Physical Vapor Deposition (PVD) Processing, Vol. 2, William Andrew, 2010.

[7] Y. Deng, S. Yin, Y. Hong, Y. Wang, Y. Hu, G. Zou, T. Kuang, K. Zhou, Microstructures and properties of novel nanocomposite WNx coatings deposited by reactive magnetron sputtering, Appl. Surf. Sci. 512 (2020) 145508.

[8] G. Zou, Y. Hong, S. Wang, S. Yin, S. Lei, Y. Wang, H. Zhu, T. Kuang, K. Zhou, Hard and tough nitrogen doped tungsten coatings deposited by HIPAC: Microstructure and mechanical properties, J. Alloys Compd. 876 (2021) 160146.

[9] J.A. Santiago, I. Fernández-Martínez, J.C. Sánchez-López, T.C. Rojas, A. Wennberg, V. Bellido-González, J. Molina-Aldareguia, M. Monclús, R. González-Arrabal, Tribomechanical properties of hard Cr-doped DLC coatings deposited by low-frequency HiPIMS, Surf. Coat. Technol. 382 (2020) 124899.

[10] J. Muñoz-García, L. Vázquez, M. Castro, R. Gago, A. Redondo-Cubero, A. Moreno-Barrado, R. Cuerno, Self-organized nanopatterning of silicon surfaces by ion beam sputtering, Mater. Sci. Eng. R: Rep. 86 (2014) 1–44.

[11] J. Seo, D.A. Pearson, R.M. Bradley, J.-S. Kim, Nanoscale pattern formation on silicon surfaces bombarded with a krypton ion beam: Experiments and simulations, J. Phys.: Condens. Matter 34 (2022) 265001.

[12] C. Li, G. Habler, L.C. Baldwin, R. Abart, An improved FIB sample preparation technique for site-specific plan-view specimens: A new cutting geometry, Ultramicroscopy 184 (2018) 310–317.

[13] P. Sigmund, Theory of sputtering. I. Sputtering yield of amorphous and polycrystalline targets, Phys. Rev. Lett. 184 (1969) 383–416.

[14] R. Behrisch, W. Eckstein, Sputtering By Particle Bombardment: Experiments and Computer Calculations from Theshold to MeV Energies, Vol. TAP 110, Springer Berlin Heidelberg New York , 2007.

[15] A. Mutzke, A. Schneider, W. Eckstein, R. Dohmen, K. Schmid, U. von Toussaint, G. Bandelow, IPP Report SDTrimSP Version 6.00, 2019, URL https://pure.mpg.de/rest/items/item_3026474/component/file_3028154/content.

[16] W. Möller, W. Eckstein, J. Biersack, Tridyn-binary collision simulation of atomic collisions and dynamic composition changes in solids, Comput. Phys. Commun. 51 (1988) 355–368.

[17] K. Nordlund, Molecular dynamics simulation of ion ranges in the 1-100 keV energy range, Comput. Mater. Sci. 3 (1995) 448.

[18] P. Sigmund, Energy density and time constant of heavy-ion-induced elastic collision spikes in solids, Appl. Phys. Lett. 25 (1974) 169.

[19] B.M. Paine, R.S. Averback, Energy density and time constant of heavy-ion-induced elastic collision spikes in solids, Nucl. Instrum. Methods Phys. Res. B. 7-8 (1985) 666–675.

[20] D.A. Thompson, High density cascade effects, Radiat. Eff. Defects Solids 56 (1981) 105–150.

[21] M. Joe, J.-H. Kim, C. Choi, B. Kahng, J.-S. Kim, Nanopatterning by multiple-ion-beam sputtering, J. Phys.: Condens. Matter 21 (2009) 224011.

[22] J. Kim, N. Ha, J. Kim, M. Joe, K. Lee, R. Cuerno, One-dimensional pattern of Au nanodots by ion-beam sputtering: Formation and mechanism, Nanotechnology 22 (2011) 285301.

[23] A. Keller, S. Facsko, Tuning the quality of nanoscale ripple patterns by sequential ion-beam sputtering, Phys. Rev. B 82 (2010) 155444.

[24] R. Cuerno, J.-S. Kim, A perspective on nanoscale pattern formation at surfaces by ion-beam irradiation, J. Appl. Phys. 128 (2020) 180902.

[25] C. Cupak, P.S. Szabo, H. Biber, R. Stadlmayr, G. C, M. Fellinger, J. Brötzner, R.A. Wilhelm, W. Möller, A. Mutzke, M.V. Moro, F. Aumayr, Sputter yields of rough surfaces: Importance of the mean surface inclination angle from nano- to microscopic rough regimes, Appl. Surf. Sci. 570 (2021) 151204.

[26] K. Schlueter, K. Nordlund, G. Hobler, M. Balden, F. Granberg, O. Flinck, T.F. Da Silva, R. Neu, Absence of a crystal direction regime in which sputtering corresponds to amorphous material, Phys. Rev. Lett. 125 (2020) 225502.

[27] T. Yasseri, R. Kree, A Monte Carlo study of surface sputtering by dual and rotated ion beams, Nucl. Instrum. Methods Phys. Res. B. 268 (2010) 2496–2503.

[28] H. Zhang, H.-W. Zhang, L. Qiao, X.-X. Zhang, R. He, P. Wang, Erosion and deuterium retention behavior of tungsten exposed to impurity-seeded deuterium plasma, Tungsten 3 (2021) 448–458.

[29] A. Kallenbach, M. Bernert, R. Dux, L. Casali, T. Eich, L. Giannone, A. Herrmann, R. McDermott, A. Mlynek, H.W. Müller, F. Reimold, J. Schweinzer, M. Sertoli, G. Tardini, W. Treutterer, E. Viezzer, R. Wenninger, M. Wischmeier, ASDEX Upgrade Team, Impurity seeding for tokamak power exhaust: From present devices via ITER to DEMO, Plasma Phys. Control. Fusion 55 (2013) 124041.

[30] A. Kallenbach, M. Bernert, P. David, D.M. G., R. Dux, E. Fable, R. Fischer, L. Gil, T. Görler, F. Janky, R.M. McDermott, W. Suttrop, G. Tardini, M. Wischmeier, ASDEX Upgrade Team, EUROfusion MST1 team, Developments towards an ELM-free pedestal radiative cooling scenario using noble gas seeding in ASDEX Upgrade, Nucl. Fusion 61 (2020) 016002.

[31] G. Hayderer, M. Schmid, P. Varga, H.P. Winter, F. Aumayr, A highly sensitive quartz-crystal microbalance for sputtering investigations in slow ion-surface collisions, Rev. Sci. Instr. 70 (1999) 3696–3700.

[32] A. Golczewski, K. Dobes, G. Wachter, M. Schmid, F. Aumayr, A quartz-crystal-microbalance technique to investigate ion-induced erosion of fusion relevant surfaces, Nucl. Instrum. Methods Phys. Res. B. 267 (2009) 695–699.

[33] R. Stadlmayr, P.S. Szabo, H. Biber, H.R. Koslowski, E. Kadletz, C. Cupak, R.A. Wilhelm, M. Schmid, C. Linsmeier, F. Aumayr, A high temperature dual-mode quartz crystal microbalance technique for erosion and thermal desorption spectroscopy measurements, Rev. Sci. Instr. 91 (2020) 125104.

[34] G. Sauerbrey, Verwendung von Schwingquarzen zur Wägung dünner Schichten und zur Mikrowägung, Z. Phys. 155 (1959) 206–222.

[35] M.V. Moro, R. Holeňák, L. Zendejas Medina, U. Jansson, D. Primetzhofer, Accurate high-resolution depth profiling of magnetron sputtered transition metal alloy films containing light species: A multi-method approach, Thin Solid Films 686 (2019) 137416.

[36] P. Ström, D. Primetzhofer, Ion beam tools for nondestructive in-situ and in-operando composition analysis and modification of materials at the Tandem Laboratory in Uppsala, J. Instrum. 17 (2022) P04011.

[37] P. Szabo, D. Weichselbaum, H. Biber, C. Cupak, A. Mutzke, R. Wilhelm, F. Aumayr, Graphical user interface for SDTrimSP to simulate sputtering, ion implantation and the dynamic effects of ion irradiation, Nucl. Instrum. Methods Phys. Res. B. 522 (2022) 47–53.

[38] R. Behrisch, J. Roth, J. Bohdansky, A. Martinelli, B. Schweer, D. Rusbüldt, E. Hintz, Dependence of light-ion sputtering yields of iron on ion fluence and oxygen partial pressure, J. Nucl. Mater. 93 (1980) 645–655.

[39] D. Gruen, A. Krauss, M. Pellin, Effects of monolayer coverages on substrate sputtering yields, Radiat. Eff. Defects Solids 89 (1985) 113–127.

[40] G. Betz, W. Husinsky, Sputtering of metal targets under increased oxygen partial pressure, Nucl. Instrum. Methods Phys. Res. B. 13 (1986) 343–347.

[41] R. Bastasz, L. Haggmark, Hydrogen ion impact desorption of adsorbed deuterium from stainless steel, J. Nucl. Mater. 111 (1982) 805–808.

[42] S. Markelj, O.V. Ogorodnikova, P. Pelicon, T. Schwarz-Selinger, I. Čadež, Temperature dependence of D atom adsorption on polycrystalline tungsten, Appl. Surf. Sci. 282 (2013) 478–486.
[43] B. Bergsnov-Hansen, R. Pasternak, A low pressure study of non-steady state hydrogen-deuterium exchange on a molybdenum surface, Surf. Sci. 17 (1969) 402–417.
[44] N. Matsunami, T. Chinushi, N. Itoh, Nuclear reaction analysis of deuterium on stainless steel surface, J. Nucl. Mater. 128 (1984) 722–724.
[45] W. Demtröder, Experimentalphysik 1, sixth ed., Springer-Verlag Berlin Heidelberg, 2013.
[46] P. Redhead, Thermal desorption of gases, Vacuum 12 (1962) 203–211.
[47] M. Pellin, C. Young, D. Gruen, Y. Aratono, A. Dewald, Oxygen underlayer formation on titanium by "static mode" laser fluorescence and auger spectroscopy, Surf. Sci. 151 (1985) 477–502.